U.S. Department of Commerce
National Oceanic and Atmospheric Administration
National Weather Service
National Centers for Environmental Prediction
5200 Auth Road
Camp Springs, MD 20746-4304

Office Note 459

ENSEMBLE-BASED BACKGROUND ERROR COVARIANCE IMPLEMENTATIONS USING SPATIAL RECURSIVE FILTERS IN NCEP'S GRID-POINT STATISTICAL INTERPOLATION SYSTEM

Yoshiaki Sato*
NCEP Visiting Scientist on leave from Japan Meteorological Agency

Manuel S. F. V. De Pondeca†, R. James Purser,
Science Applications International Corp., Washington, D.C.

David F. Parrish
Environmental Modeling Center, Camp Springs, Maryland

June 2009

.

* Email: y-sato@met.kishou.go.jp
† Email: Manuel.Pondeca@noaa.gov

Abstract

A methodology for specifying ensemble-based background error covariances within the recursive-filter (RF) formalism of the NCEP Grid-point Statistical Interpolation (GSI) is proposed and tested using a low-resolution version of the North-American Regional Data Assimilation System. Perturbation fields from six-hour forecasts from the 80-member NCEP Global Ensemble Forecast System are used to represent the background errors. The RF-generated covariances are found to agree fairly well with the exact covariances computed directly from the ensemble perturbation fields in the vicinity of the selected test points. In addition, they are necessarily free of the spurious correlations at long ranges that characterize the covariance-matrix of the low-dimension space of the sample ensemble perturbations. The anisotropies are found to be rather weak when the 80-member ensemble is used without any further treatment to prescribe the local aspect tensor required by the recursive filter. However, a remarkable enhancement of the anisotropy is obtained when the ensemble size is artificially increased through a special type of local averaging. Results from a case study reveal an improvement of the 500 hPa geopotential height skill scores when the convariances with enhanced anisotropy are applied.

1. Introduction

An important component of a variational data assimilation is the assumed background error covariance matrix **B** as it determines the manner in which the information from the observation increments is spread to the nearby grid points and model variables that may not be a direct part of the observation operator (Daley 1991). **B** is a very large, positive semi-definite matrix, which contains in excess of 10^{12} independent elements in most assimilations used to initialize modern-day atmospheric models. The impracticability of storing such a large matrix is usually overcome by recognizing that it suffices to the assimilation system to access a "recipe" that delivers the vector product **x=Bf** given any vector of forcings **f**. However, the lack of computationally feasible methods to implement adaptive and realistic flow-dependent covariances has for a long time restricted the assimilation to using simplifying assumptions of homogeneity and isotropy for the background errors. The approach typically decomposes **B** into a set of univariate covariance matrices of carefully selected analysis variables for which these assumptions are more easily justified. Error correlations across variables are then partially accounted for by imposing additional balance constraints on the analysis increments for the separate analysis variables. Furthermore, it is common to assume Gaussian-shaped profiles for the covariances of background errors, a choice which is at times solely motivated by their attractive analytical and numerical properties.

In recent years, several efforts have been documented that seek to relax the isotropic assumption for the background errors. Riishøjgaard (1998) proposes a methodology for mapping the covariances to a selected background field (see also Liu et al 2007). The approach augments the original Gaussian isotropic covariance function with a new multiplying Gaussian factor expressed in terms of the spatial gradients of the background field and a "function correlation length" that controls the strength of the anisotropy. Desroziers (1977) suggests that the assumption of an isotropic covariance in the geostrophic momentum space of the semi-geostrophic theory (Hoskins and Bretherton 1972, and Hoskins 1975) translates into the desired anisotropic covariance in real-space. His examples display covariances in real-space that stretch along frontal-boundaries and contract across the same boundaries. Another approach is to use the background error estimated by an Ensemble Kalman Filter (EnKF). Hamill and Snyder (2000) test a hybrid system of the EnKF and three-dimensional variational (3Dvar) assimilation, and Buehner (2005) uses the EnKF-derived background error in a 3Dvar assimilation. The use of spatial recursive filters to simulate the convolution of forcings by the background error covariances, as is done at the National Centers for Environmental Prediction (NCEP), offers yet another

elegant and computationally efficient means by which to synthesize flow-dependent covariances. In the simplest case, where the covariance is modeled using a single quasi-Guassian component, the most basic parameters of the adaptive covariances are the amplitude (i.e., the variance) and the components of the aspect tensor at each grid point. The versatility of the method is illustrated by De Pondeca et al. (2006), who implement variants of the original Riishøjgaard and Desroziers models. These authors also expand the Desroziers model to include an isentropic vertical coordinate (Hoskins and Draghici 1977), and propose a novel covariance construction based on the concept of kinematic deformation at finite time lag. In fact, the Desroziers and kinematic method can, in a broader sense, be regarded as variants of the Riishøjgaard method for different choices of anisotropy-forcing variables.

While the methods illustrated by De Pondeca et al. (2006) are able to provide stretching parameters for obtaining useful anisotropic covariances, none of them adequately addresses the issue of inferring the covariance amplitudes from the background field, or the separate problem of modulating their prescriptions of anisotropy and amplitude to take into full account the varying influence upon background error quality of the previous cycles of measurements. It would seem that, using the background field itself, there is simply not enough information from which to deduce the background error variance, or the subtle details about the way the distribution of previous measurements would have influenced the anisotropy of the covariances of the errors of this background. The dispersion of the members of the ensemble of up-to-date forecasts could redress these omissions by supplying vital information about how uncertain the background errors are, and how correlated they are likely to be at different orientations. This work expands that of De Pondeca et al. (2006) to explore the use of the NCEP Global Forecast Ensemble to specify the background error covariances in a regional data assimilation.

The text is organized as follows: Section 2 highlights features of the NCEP data assimilation system that are most relevant to this work, and presents the ensemble-based covariance formulation. Section 3 describes the low-resolution regional data assimilation system used to test the ensemble-based covariances, and section 4 presents the results. The summary and discussion are found in section 5.

2. The Assimilation System and the Ensemble-Based Background error Model

(a) Notes on the Grid-point Statistical Interpolation

NCEP uses the Grid-point Statistical Interpolation (GSI) for both regional and global data assimilations. The GSI is a 3Dvar system formulated in the model grid space (Wu et al. 2002), whereby the action of the background error covariances is simulated with the help of spatial recursive filters. The use of recursive filters in the GSI parallels the multiple iteration of a diffusion operator to produce Gaussian covariances (Derber and Rosati 1989, and Weaver and Courtier 2001). However, it takes less iterations to produce the desired Gaussian kernels with the recursive filters than are required by the explicit use of a diffusion operator. The operational GSI uses univariate, horizontally isotropic background error covariances which are generated by applying the recursive filters along each grid coordinate direction. The 3Dvar is incremental and uses the following set of perturbations as its analysis variables: stream function, unbalanced parts of (i) velocity potential, (ii) temperature, and (iii) surface pressure, and pseudo-relative humidity, skin temperature, cloud water, and ozone. The balance relationship is based on a regression approximation to geostrophy.

When combined with the line-filtering "hexad" algorithm, a special class of recursive filters now available to the GSI is capable of simulating anisotropic covariances of any given shape as defined by the spatially smooth local aspect-tensor of spatial dispersion (Purser et al, 2003a,b, Purser 2005, and Purser et al. 2007). The grid-space formulation of the analysis system in conjunction with the use of these filters provides a large flexibility for the background error specifications. It enables the user to consider the atmospheric condition in the physical space and directly account for the flow-dependency in the covariance construction without any need for auxiliary coordinate transformations.

(b) Formulation of the Ensemble-based Covariance Model

The recursive filters of the GSI assume Gaussian models of auto-covariance. They use as input parameters the background error variance and the local aspect tensor at each grid point. The inverse of the latter takes the following form for the quasi-isotropic model:

$$A_{iso}^{-1} = diag\left\{L_h^{-2}, L_h^{-2}, L_v^{-2}\right\} \quad , \tag{1}$$

where L_h and L_v, are the horizontal and vertical correlation lengths, respectively.

Suppose P is a field of perturbation of a quantity we intend to assimilate and let an ensemble of N members supplying realizations of short forecasts of P be available. Let overbars denote the ensemble expectation operator. Assume the mean has already been removed from the ensemble whose members are otherwise independent (and therefore collectively possess N-1 degrees of freedom at every grid point). Attempts to use the general ensemble covariance,

$$\hat{B} = \frac{1}{N-1}\sum_{\alpha=1}^{N} \mathbf{P}_\alpha \mathbf{P}_\alpha^T = \overline{\mathbf{P}\mathbf{P}^T} \quad , \tag{2}$$

directly to assimilate new data are always compromised by the appearance of spurious features at long-range that come from inadequate sample sizes. Indirect approaches, where the spurious covariances at long-range are artificially suppressed, introduce artifacts of their own, especially at larger scales of increments. However, the sample variance of the quantity at each grid point x:

$$\overline{P(x)^2} = \frac{1}{N-1}\sum_{\alpha=1}^{N} P_\alpha(x)^2 \quad , \tag{3}$$

is much better defined, being a single value per grid point and much less subject to the debilitating effects of sampling errors (even though they still come into play in this estimate). Similarly, a sample estimate of the covariance, in situ, of the gradient of *P(x)*, as given by:

$$\overline{\nabla P(x)(\nabla P(x))^T} = \frac{1}{N-1}\sum_{\alpha=1}^{N} \nabla P_\alpha(x)(\nabla P_\alpha(x))^T \quad , \tag{4}$$

provides only a handful of values per grid point and is therefore unlikely to suffer from the more serious manifestations of sampling problems. Nevertheless, it is recommended that even these estimates be used in conjunction with other information to maximize their overall utilization. For example, based upon experience from the "climatology" of forecast errors, which can supply estimates, $\left\langle P_0^2(x)\right\rangle$ and $\left\langle \nabla P_0(x)(\nabla P_0(x))^T \right\rangle$, we can use these to "dilute" the ensemble sample estimates in order to make the latter more robust, and write:

$$\left\langle P_{new}^2(x)\right\rangle = (1-W)\left\langle P_0^2(x)\right\rangle + W\overline{P^2} \quad , \tag{5}$$

and

$$\left\langle \nabla P_{new}(x)(\nabla P_{new}(x))^T \right\rangle = (1-W)\left\langle \nabla P_0(x)(\nabla P_0(x))^T \right\rangle + W\overline{\nabla P(x)(\nabla P(x))^T} \quad , \tag{6}$$

where W < 1 denotes the proportionate weight assigned to the ensemble. Now we are in a position to estimate the local aspect tensor, $\boldsymbol{A}$, for the quasi-Gaussian covariance model for P with a significant input from the ensemble. The simplest way is to define, at each grid point:

$$\mathbf{A}^{-1} = \frac{\left\langle \nabla P_{new}(x)\left(\nabla P_{new}(x)\right)^T \right\rangle}{\left\langle P_{new}^2(x) \right\rangle} \quad . \tag{7}$$

A simple and trivial variant of this formulation empirically adds the ensemble contribution to the already existing isotropic inverse aspect tensor, to obtain:

$$A_{ani}^{-1} = \alpha A_{iso}^{-1} + \beta \frac{\overline{\nabla P(x)(\nabla P(x))^T}}{\overline{P(x)^2}} \quad , \tag{8}$$

where α and β are calibrating parameters determined by trial and error.

These techniques may not be the final answer. For example, they must necessarily be modified in the cases of more sophisticated covariance models synthesized from multiple quasi-Gaussian components. However, they do obtain from the ensemble precisely the quantities needed by the existing recursive filtering codes to enable stretched adaptive covariances to be used with a reasonable assurance of realistic amplitudes and shapes.

The results reported in this work are based on equation (8), with $\alpha = 5/6$ and $\beta = 1$.

3. The low-resolution data assimilation testbed

The NCEP operational regional data assimilation system, which comprises the GSI and the North American Mesoscale (NAM) model run at 12-km resolution, is commonly known as NDAS. For this study, we used a lower-resolution, 48-km version of the NDAS, hereby abbreviated as LR-NDAS. Its model domain and topography are shown in Fig. 1. The number of grid points in the east-west and north-south direction are 303 and 267, respectively, which are about 1/4 of those used by the operational NDAS (1211x1067) before the 2008 change to use an extended domain. The vertical resolution and the number of vertical levels (60) are the same as in the operational NDAS. The first guess and the lateral boundary conditions for the GSI are taken from the operational NCEP Global Forecast System (GFS). Just as with its operational counterpart, the LR-NDAS is designed to perform 12-hour assimilation cycles followed by up to 84-hour free forecasts. The 12-hour cycle is broken into four pieces: a 3Dvar analysis with a subsequent 3-hour forecast which provides the first guess for the next analysis.

In order to evaluate the performance of the LR-NDAS, we conducted a 12-hour data assimilation cycle from 12 UTC 19 June 2007, and compared the analysis fields and analysis increments from the last data assimilation with the corresponding results using the operational NDAS. The observations used were the same for the LR-NDAS and the operational NDAS. For both systems, Fig. 2 displays the analyzed temperature and temperature increments at the model level 40 (~500 hPa). We witness a good agreement between the results from both systems especially in their large scale features. Qualitatively similar results were also obtained for other model levels and variables. These findings are very encouraging, especially on account of the fact that we performed the evaluation at the end of the four-piecewise 12-hour assimilation cycle. The results show that

the LR-NDAS, which uses much less computational resources than required by the operational NDAS, can provide us with useful data assimilation and forecast results for time efficient research.

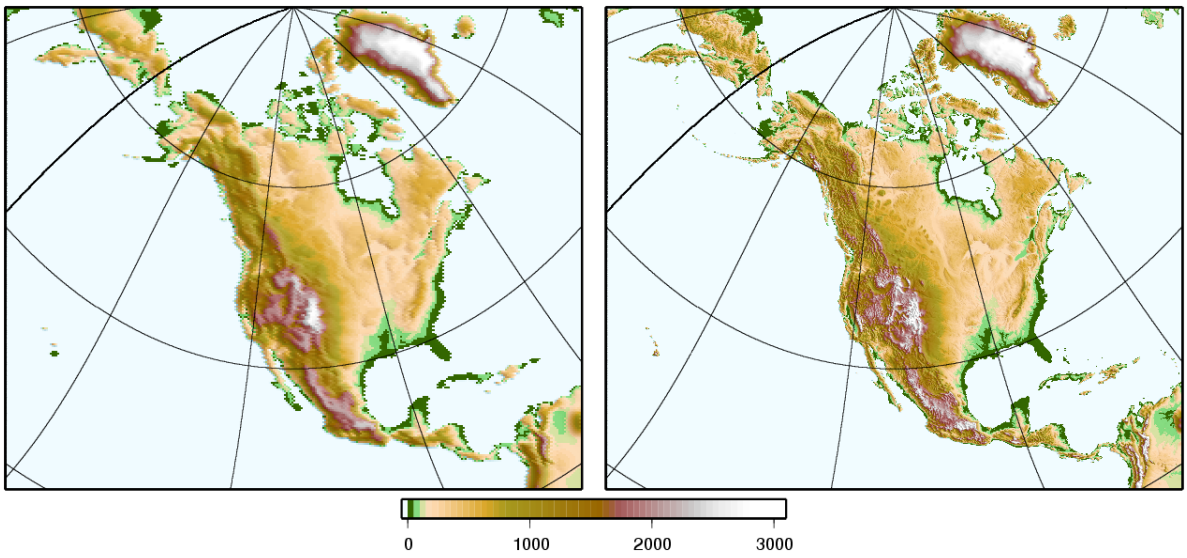

Fig. 1: Model domain and topography in meters for LR-NDAS (left panel) and operational NDAS (right panel). To emphasize the orography, the color is shaded by a 45 degree lighting angle. As expected, LR-NDAS displays a smoother topography than NDAS.

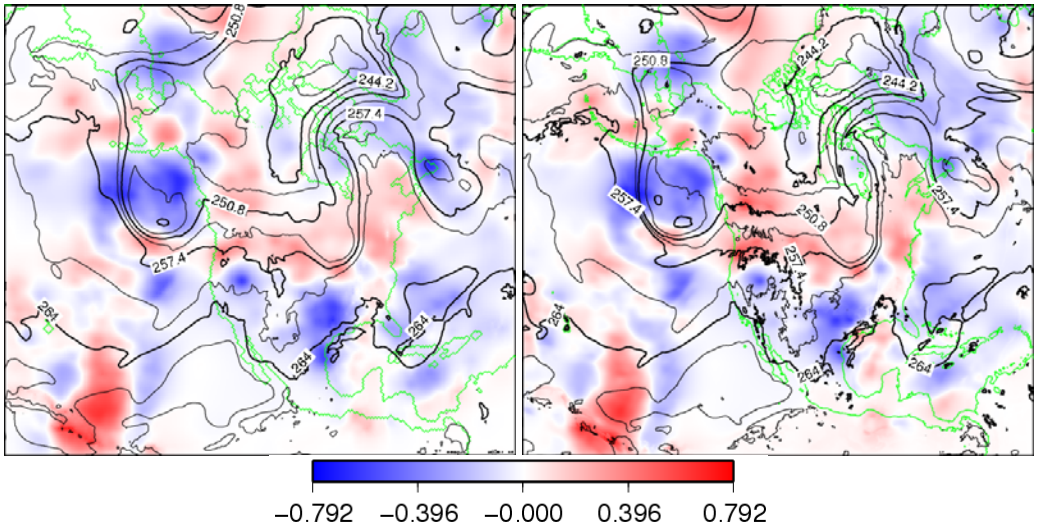

Fig. 2: Analyzed temperature in K (contour lines) and temperature increments also in K (color scales) at model level 40 (~500 hPa) in the last analysis of the 12-hour data assimilation cycle. Left panel for LR-NDAS and right panel for operational NDAS. The valid time is 00 UTC 20 June 2007.

4. Results

(a) The ensemble-covariance shapes

We used six-hour forecasts from the NCEP Global Ensemble Forecast System (Wei et al. 2008) with the mean removed to build the background error covariances. These fields were interpolated to the A-grid of the GSI and converted to the form of the analysis variables. In particular, a two-dimensional fast-Fourier transformation was applied in order to derive stream function and velocity potential from the original U and V-wind components of the ensemble perturbation fields. The fields on the A-grid were smoothed using a five-point smoother prior to their use to estimate the elements of the aspect tensor.

Using an 80-member ensemble, Figs. 3 and 4 compare the RF-based estimates of the stream function auto-correlations obtained via eq. (8) with the auto-correlations computed directly from the ensemble using eq. (2). The results are shown for 20 selected points on the analysis grid. Since the GSI estimation uses only the gradient of the ensemble perturbation fields, it does not come as a surprise that the shapes of the ensuing auto-correlations do not always match those from the exact sample auto-correlations very well. But roughly speaking, the shapes display reasonable similarities. For example, the covariance for point **b** in Fig. 3 shows a triangular shape with a narrow upper half and a fat bottom half. The 0.8 contour line of the corresponding exact sample ensemble perturbation auto-correlation in panel **B** of Fig. 4 displays similar characteristics. Figures 3 and 4 also show that both computations lead to a good agreement in the relative spatial reach of their covariances. On an additional positive note, it is also important to stress the absence of spurious long-range correlations in the GSI estimations. Spurious correlations are, however, clearly seen in Fig. 4 at large distances from the anchor points as a result of sampling errors. Finally, we note that both figures show rather weak anisotropies. We address this issue at a later stage.

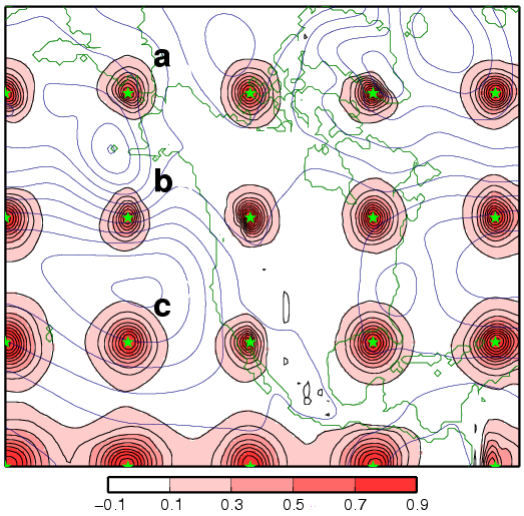

Fig. 3: Color scales (and black contours at 0.1 contour interval) show the GSI estimated auto-correlation for stream function computed via eq. (8) for 20 selected points at model level 5 (~1010 hPa). The selected points are denoted by a green star symbol. Blue contour lines show the stream function in the input guess field as a reference. Actual values are of no consequence. The valid time is 18 UTC 26 December 2007.

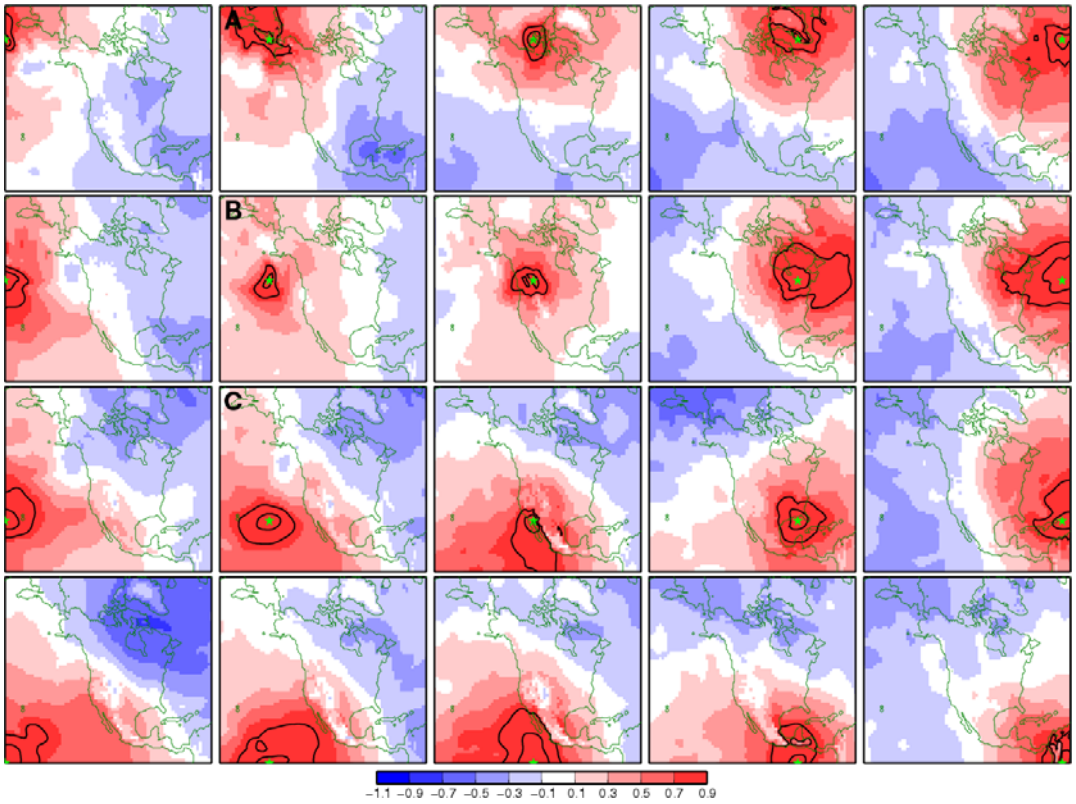

Fig. 4: As in Fig. 3, but computed directly from the ensemble perturbation fields using eq. (2). Each panel shows the auto-correlation field against the anchor points indicated by a "green star." The order of the panels corresponds to that of the signal points in Fig. 3. For example, the estimated covariance "a" in Fig. 3 is to be compared to that of the panel A in Fig. 4, covariance b to panel B, and so on. Red color indicates positive correlation and blue color negative correlation. Solid lines display the 0.8 and 0.95 auto-correlation levels.

(b) Comparison of the 80 member with the 20 member Global Ensemble (GENS)

Although the NCEP Global Ensemble Forecast System uses an 80-member ensemble (GENS80) during its data assimilation cycling, only a 20-member ensemble (GENS20) is available for the full duration of the free forecast. If we are to use the output from this system to build ensemble-based covariances in the real-time NDAS, it thus becomes important to assess how the GSI estimated covariances change when using the reduced 20-member ensemble. We start by comparing the ensemble forecast spreads from GENS20 with those from GENS80. For surface pressure, Fig. 5 shows the six-hour spread, and Fig. 6 displays similar results for temperature at model level 40 (~ 500 hPa). For both fields, we find a very good overall agreement between GENS20 and GENS80, although the fields are slightly smoother for GENS80.

Secondly, we show in figures 7a and 7b the auto-correlations computed directly from the ensemble perturbations using eq. (2) for nine selected anchor points, indicated by a "green star" on each panel. As expected, GENS20 shows more spurious correlations at long distances from the anchor points than we see for GENS80. However, it is important to note that the extent and shape of the region of strong correlation in the vicinity of the anchor point is fairly similar for GENS20 and GENS80. As a result, the corresponding GSI estimated covariances, which are displayed in Fig. 8, show similar shapes. The conclusion is fairly similar for temperature (see Figs. 9a, 9b, 10a and 10b).

The above comparisons show that the GSI can estimate the ensemble covariances reasonably well even with a 20 member ensemble, although it would certainly be preferable to use a larger ensemble.

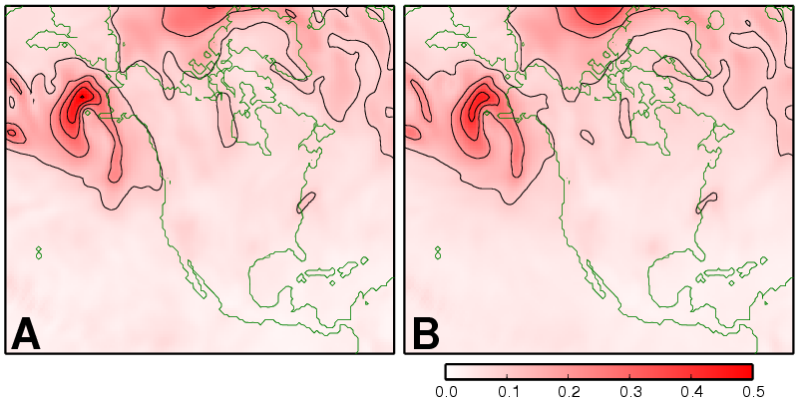

Fig. 5: Six-hour ensemble forecast spread for surface pressure over the LR-NDAS domain in hPa. The valid time is 18 UTC 26 December 2007. Panel A for the 20 member GENS and B for the 80 member GENS.

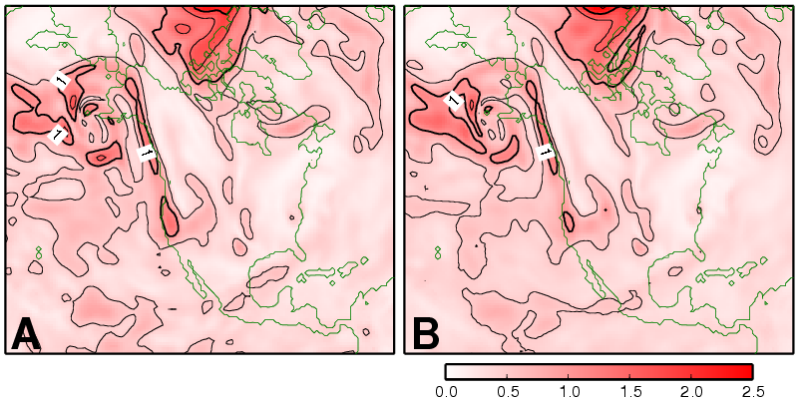

Fig. 6: Same as in Fig. 5, except for temperature in K at model level 40, which corresponds to approximately 500 hPa.

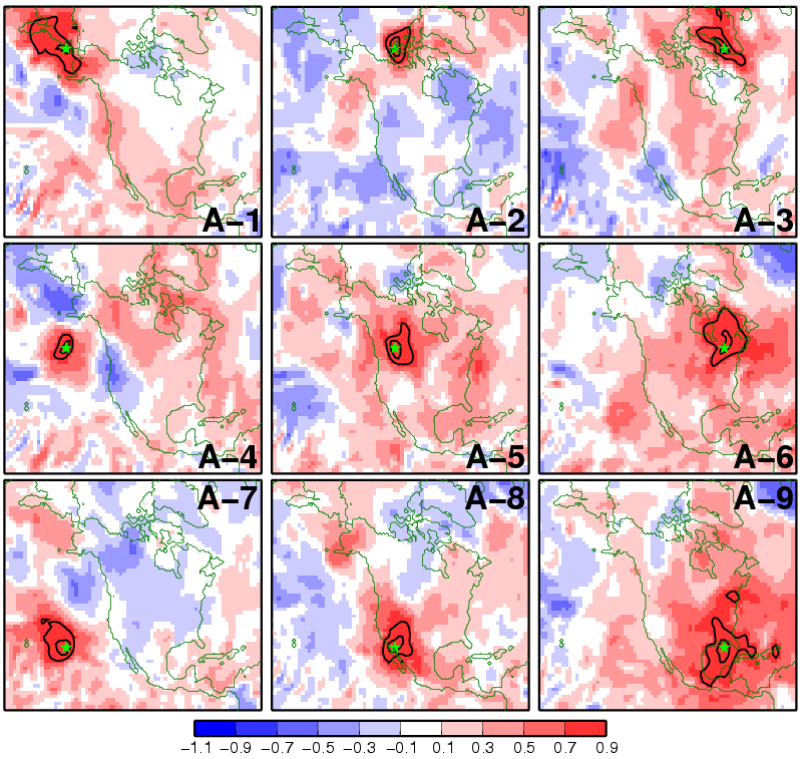

Fig. 7a: For GENS20, the ensemble forecast perturbation auto-correlations for the nine points indicated by the "green star" points computed using eq. (2). Solid contours represent the 0.8 and 0.95 levels.

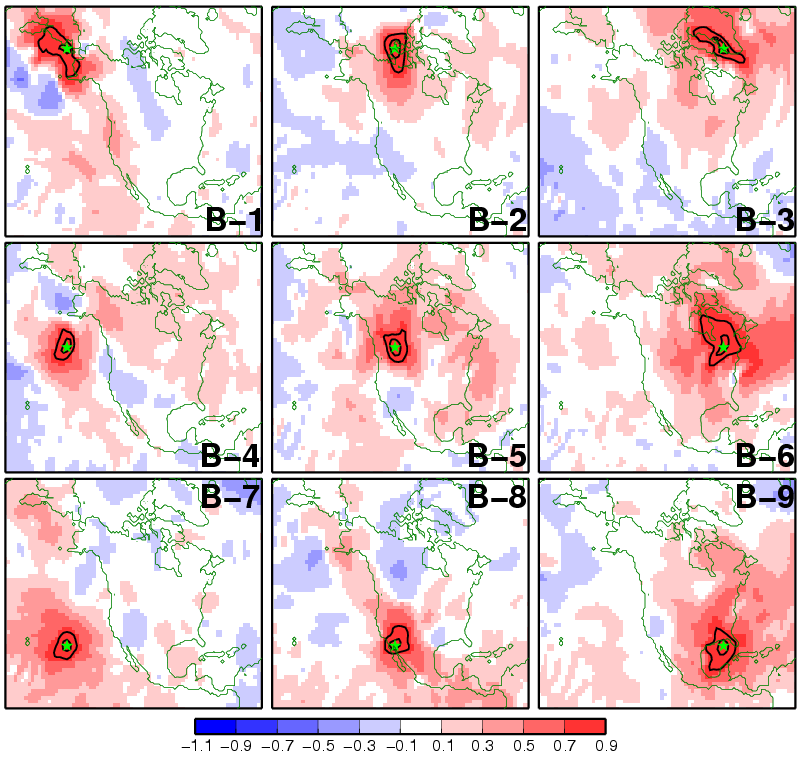

Fig. 7b: Same as in Fig. 7a, but for GENS80.

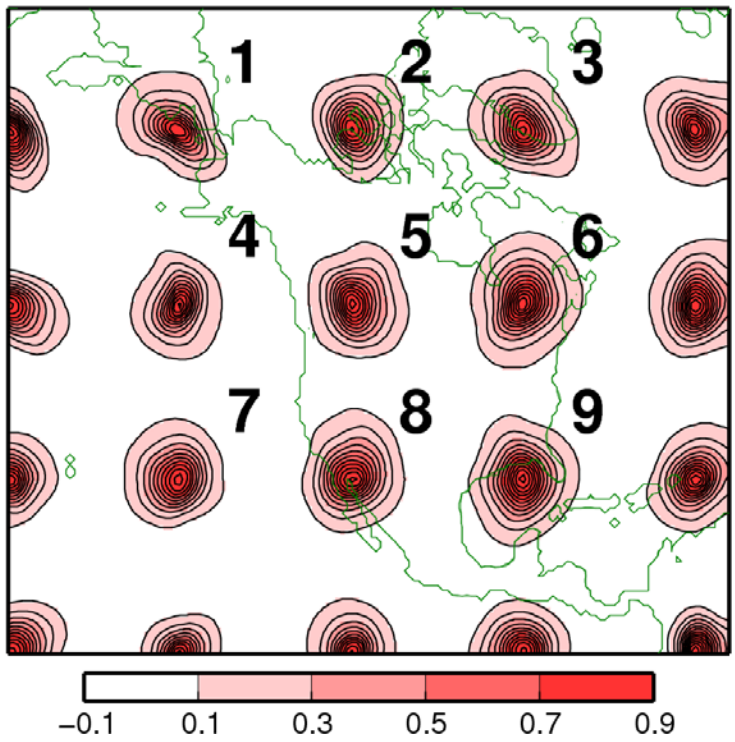

Fig. 8a: For GENS20, the GSI estimated auto-correlation for surface pressure for the nine points of Fig. 7 computed via eq. (8).

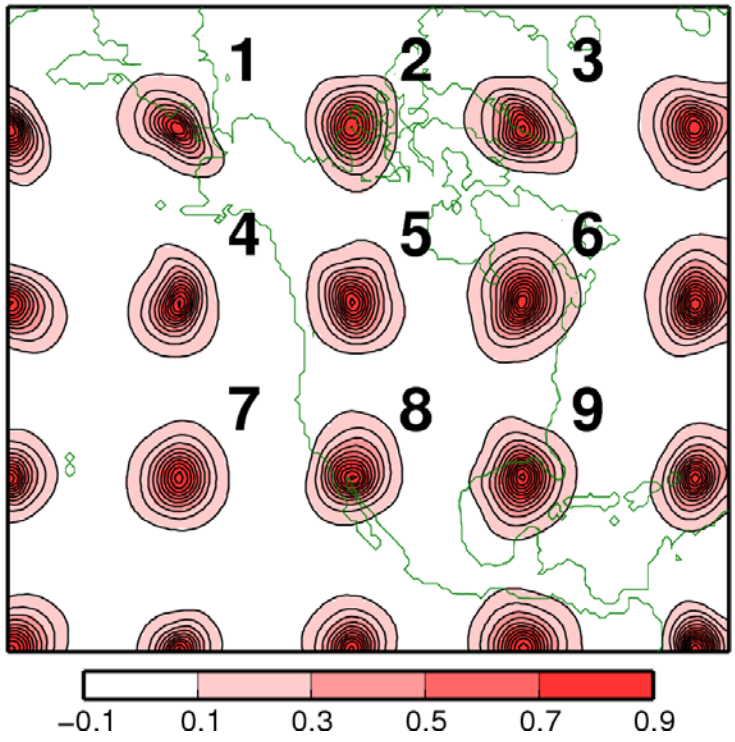

Fig. 8b: Same as in Fig. 8a, but for GENS80.

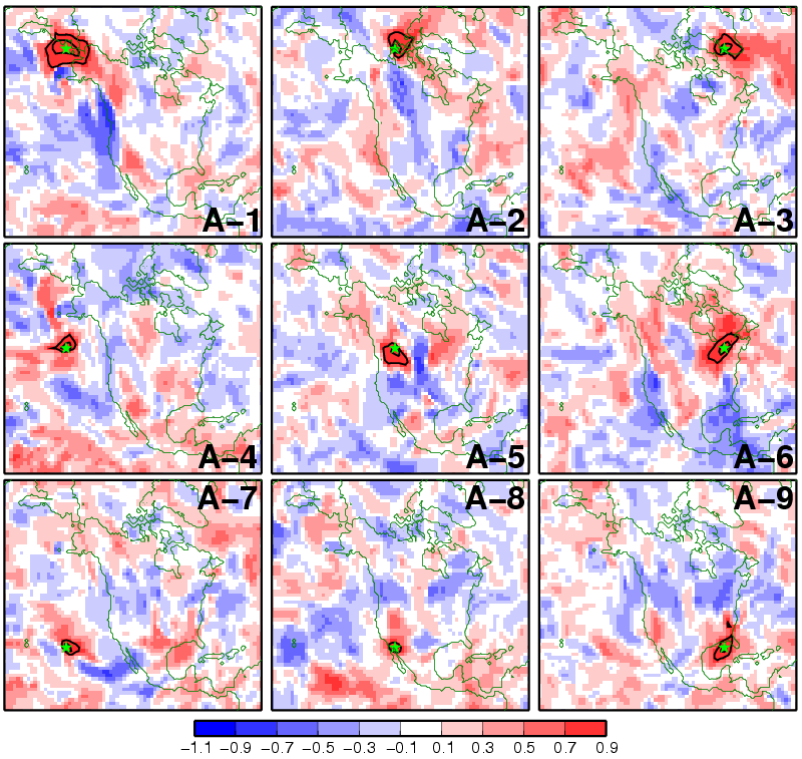

Fig. 9a: Same as in Fig. 7a but for temperature at model level 40 (~500 hPa)

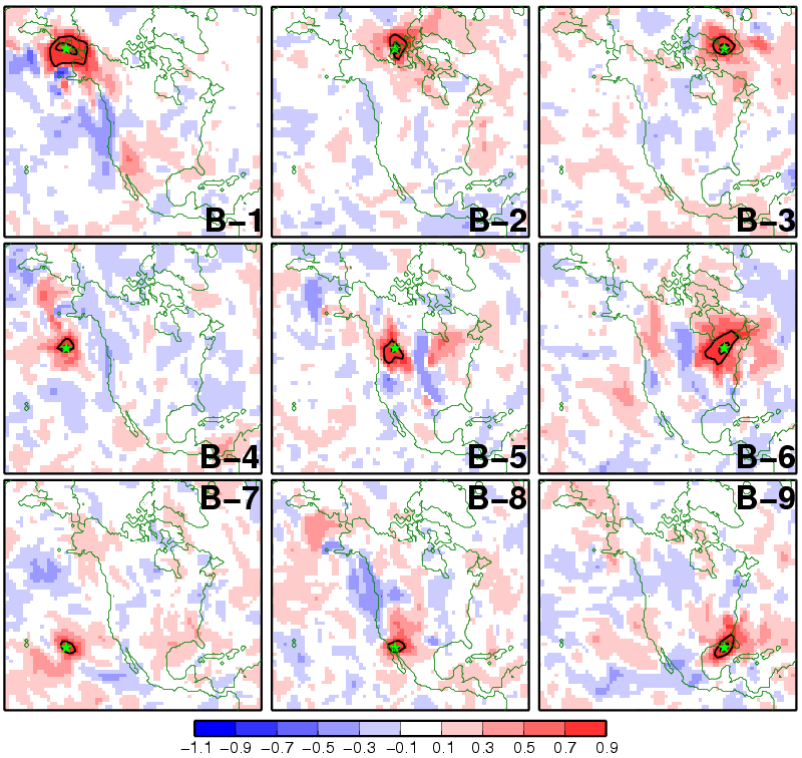

Fig. 9b: Same as in Fig. 7b but for temperature at model level 40 (~500 hPa)

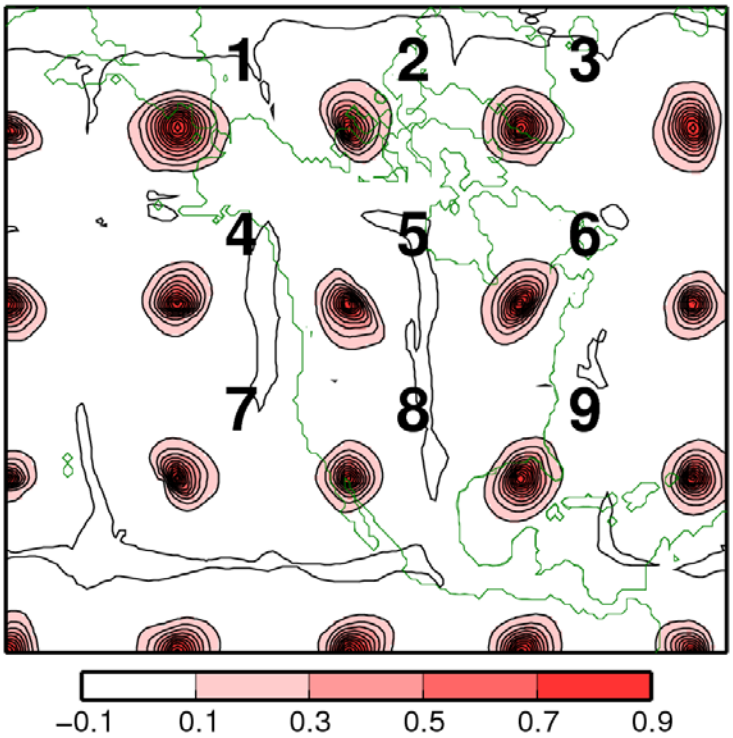

Fig. 10a: Same as in Fig. 8a but for temperature at model level 40 (~500 hPa)

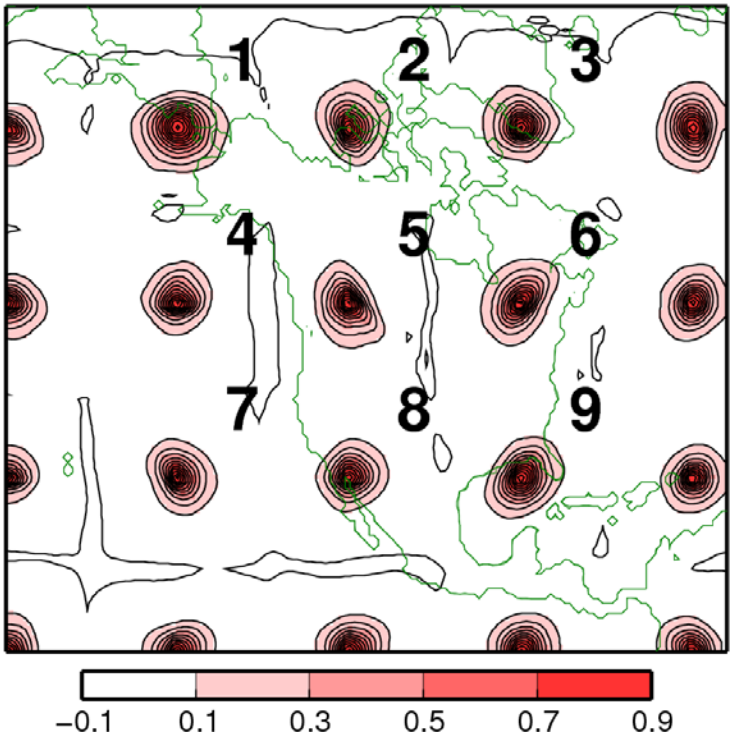

Fig. 10b: Same as in Fig. 8b but for temperature at model level 40 (~500 hPa)

(c) Enhancing the anisotropy by artificially increasing the sample size.

Although eq. (8) leads to correlation shapes that compare fairly well with those from the exact ensemble perturbation correlation, we found the anisotropy to be weak. Therefore, we tried to enhance the anisotropy by introducing an additional gradient-like term in the covariance model formulation. This was done by composing a "new," augmented ensemble at each grid point with the help of the information from the surrounding points. The original idea is described in Berre et al (2007). That is, we assume that the horizontally surrounding 8 grid point data in Fig. 11 are members of the center grid "0" ensemble. With this treatment, we can increase the ensemble size by a factor of 9. We show next how the new ensemble perturbation components are represented by the original ensemble perturbations.

1	2	3
4	0	5
6	7	8

Fig. 11: Target grid (0) and surrounding 8 grids (1~8)

Suppose M_j is the mean of the original full ensemble fields for grid *j*. Then, the new ensemble mean for grid 0 ($\widetilde{M}_0$) will be:

$$\widetilde{M}_0 = \frac{1}{9}\sum_{j=0}^{8} M_j \quad . \tag{9}$$

The original ensemble perturbation of member *m* at grid *j* (P_{jm}) is represented as follows, using the full grid value (D_{jm}) and the ensemble mean (M_j):

$$\left\{P_{jm}\right\}_{m=1\sim N} = \left\{D_{jm} - M_j\right\}_{m=1\sim N} \quad , \tag{10}$$

where N is the size of the ensemble. Using eq. (10), the new ensemble perturbation of member *m* at grid 0, originated from grid *j* ($\widetilde{P}_{0jm}$) should then be written as follows:

$$\left\{\widetilde{P}_{0jm}\right\}_{m=1\sim N,\, j=0\sim 8} = \left\{D_{jm} - \widetilde{M}_0\right\}_{m=1\sim N,\, j=0\sim 8} = \left\{P_{jm} + \left(M_j - \widetilde{M}_0\right)\right\}_{m=1\sim N,\, j=0\sim 8} \quad . \tag{11}$$

Therefore, the size of $\widetilde{P}_{0jm}$ is $9N$ as already stated, and it is also important to note that $\widetilde{P}_{0jm}$ contains the gradient-like term $\left(M_j - \widetilde{M}_0\right)$ which serves to enhance the anisotropy.

The results of our first test using equation (11) display very steep anisotropy as shown in Fig. 12. This appears to originate from the large grid interval used in the LR-NDAS in conjunction with the fact that distances are specified in grid units when computing field gradients for the aspect tensor. We note the strong "background following-character" of the covariances, which is characteristic of the Riishøjgaard method. This suggests that the mean-field gradient-like term in (11) is the dominant term. We therefore introduce a rescaling coefficient $C_{rg}\left(=1/8\right)$ to reduce the impact of this gradient-like term:

$$\left\{\widetilde{P}_{0jm}\right\}_{m=1\sim N,\, j=0\sim 8} \equiv \left\{P_{jm} + C_{rg}\left(M_j - \widetilde{M}_0\right)\right\}_{m=1\sim N,\, j=0\sim 8} \quad . \tag{12}$$

We note that the above factor 8 is a "guess" that reflects the LR-NDAS horizontal resolution ratio of 4 compared to the operational NDAS, and an additional ratio of 2 that accounts for the fact that the anisotropic filter is in fact applied on a lower resolution space compared to that of the analysis grid.

The results with the new formulation (12) are also shown in Fig. 12. Although what the desirable amount of anisotropy should be remains an open question, the new equation (12) seems to yield acceptable results. At least they suggest that C_{rg} could be successfully used to calibrate the covariance model to achieve optimal forecast results under a chosen verifying metric.

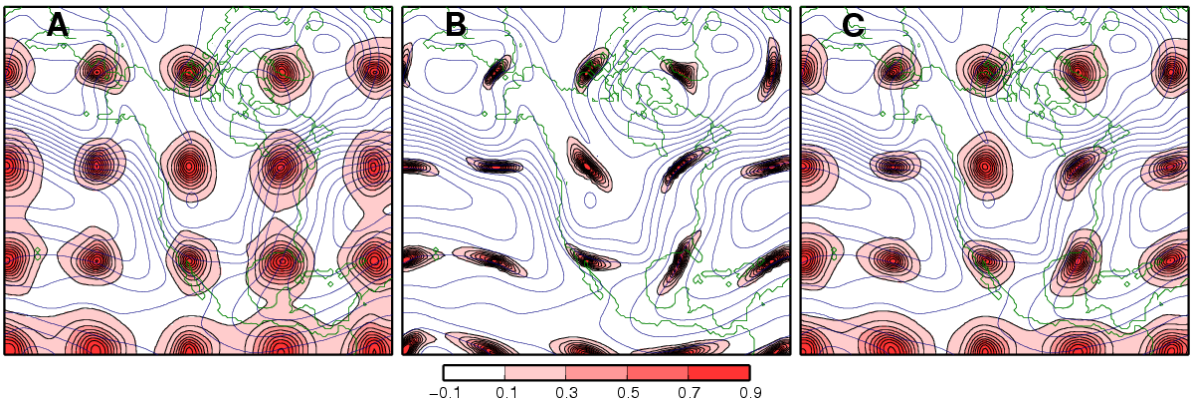

Fig. 12: The GSI estimated auto-correlation for 20 selected points (color scales and black contour lines with the interval of 0.1). Panel A for the GSI default isotropic model, B for covariance model of eq. (11), and C for covariance model of eq. (12) perturbation. Blue contour lines show the stream function for the first guess field as a reference. Actual values are of no consequence.

(d) Data assimilation and forecast results

We conducted a set of four experiments comprising a single data assimilation followed by a free 72-hour forecast. The initial time was 18 UTC 26 December 2007. The configuration of the data assimilation for each test was as follows: The benchmark experiment g2iso used the default isotropic recursive filter of the GSI; experiment g2aiso0 the anisotropic recursive filter, but set to simulate isotropic covariances; experiment g2ens80-1 used the 80-member ensemble-based covariances; and experiment g2chk0 the "surrounding grid augmented" 80-member ensemble-based covariances. In g2ens80-1 and g2chk0, the anisotropy was only applied to the stream function and velocity potential. Fig. 13 shows the wind speed analysis and analysis increments at model level 50 (~240 hPa) for all four configurations. We see that g2aiso0 leads to forecast results that agree reasonably well with those obtained with the default isotropic model (g2iso). This is an important aspect, since the assimilations in these two experiments use different implementations of the recursive filters. In particular, the isotropic filter of the default GSI applies the horizontal covariances separately from the vertical covariances, while the anisotropic filter does not perform such a separation. Hence, before any truly anisotropic experiments are performed, it would be desirable to calibrate the anisotropic filter to simulate the isotropic case in a manner that is comparable to the results from the benchmark experiment. Fig. 13 also shows that the impact of the ensemble-based covariance model in the g2ens80-1 experiment is very limited. The results from g2ens80-1 differ very little from those of g2aiso. The g2chk0 experiment, in its turn, leads to a strong anisotropy, with analysis increments stretched along the jet axis. Qualitatively similar results are obtained at other model levels.

We evaluated the performance of our experiments by computing the 500 hPa geopotential height skill scores (SS) (see Wilks 1995):

$$SS(t) = 1 - \frac{MSE(t)}{MSE_{control}(t)} \quad . \tag{13}$$

$MSE_{control}(t)$ represents the mean-squared errors for the control forecast, taken to be that of the g2iso experiment, and $MSE(t)$ are the mean-squared errors for g2aiso0, g2ens80-1, or g2chk0. The errors were computed at 12-hour intervals with respect to the operational 12-km forecast, taken to represent the "truth." In equation (13), " t " denotes the forecast time. Positive (negative) values of the SS indicate improved (degraded) forecasts with respect to the control, which is characterized by $SS(t) = 0$. The upper bound for this forecast measure is $SS(t) = 1$, which corresponds to a perfect forecast, while the lower bound is theoretically $(-\infty)$.

Fig. 14 shows that the direct use of the 80-member ensemble as is done in g2ens80-1 slightly degrades the forecast. However, the figure also shows a much improved forecast when the ensemble size is artificially increased by using information from surrounding grid points (experiment g2chk0). This is the experiment that displayed the strongest anisotropy in the analysis increments.

For the benchmark experiment, Fig. 15 displays the 500 hPa geopotential height forecast field at 24-hour intervals on the AWIPS grid 212, which is a 40-km resolution Lambert Conformal grid covering the conterminous USA. For reference, it also displays the corresponding fields from the operational NAM analysis, which we take to represent the "truth." As expected, the deviation of the benchmark forecast from the "truth" increases with the forecast time. In order to better highlight the differences between the various experiments with the anisotropic filter, we computed difference fields with respect to the benchmark experiment rather than the "truth." The resulting difference fields are also displayed in Fig. 15. We see that, while the evolution of the difference fields is very similar for experiments g2aiso0 and gens80-1, it is remarkably different for g2chk0. Further work is needed to understand the dynamic of this case, but it would appear that the decrease of the mean-squared errors in g2chk0 comes from the smaller errors over the Hudson Bay at the initial forecast time. We must note, however, that similar initial error reductions were not found at the lower model levels (not shown).

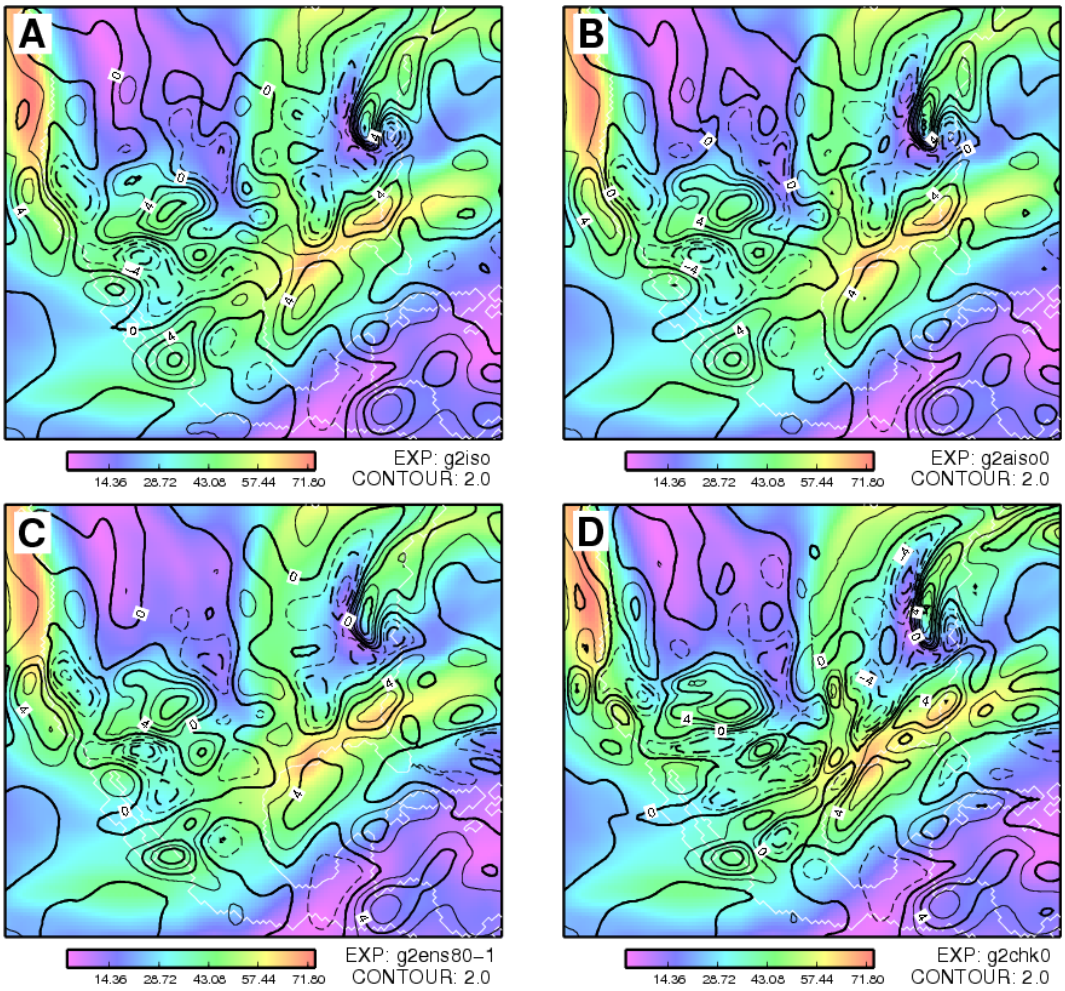

Fig. 13: The wind speed analysis in m/s (shaded contours) and analysis increments (contour lines at 2m/s interval) at model level 50 (~240 hPa) using (A) the default isotropic filter (g2iso), (B) the anisotropic filter simulating the isotropic mode (g2aiso0), (C) the 80-member ensemble based anisotropy (g2ens80-1), and (D) the "surrounding-grid points augmented" 80-member ensemble based anisotropy (g2chk0). The analysis time is 18 UTC 26 December 2007.

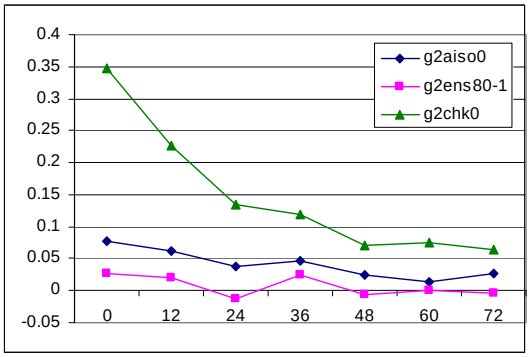

Fig. 14: The 500 hPa skill-scores for experiments g2aiso0, g2ens80-1, and g2chk0, using g2iso as the control forecast (see also Fig. 13).

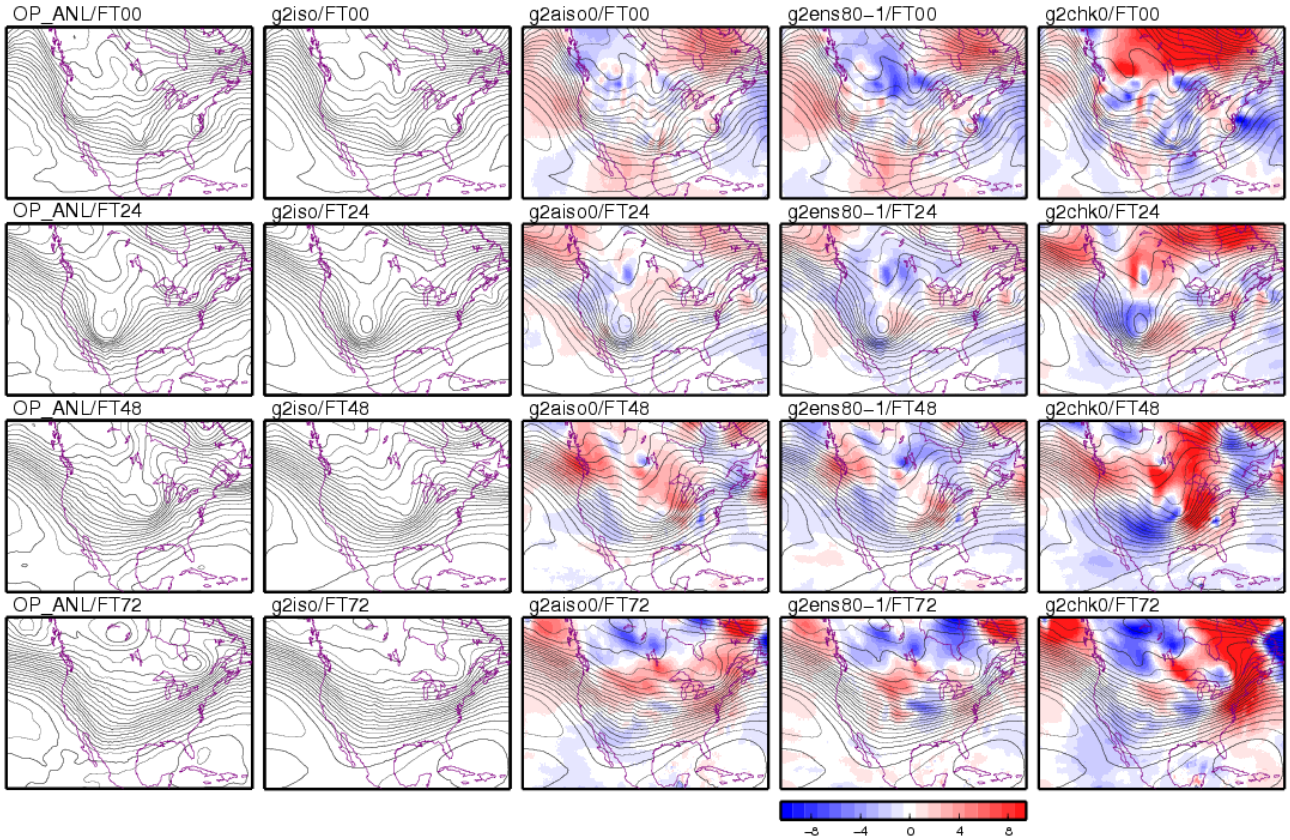

Fig. 15: The 500 hPa geopotential height analysis patterns from the operational NAM (first panels from left), and from the control experiment g2iso (second panels from left) at 12 hour interval. The color shades in the third, fourth, and fifth panels from left display the 500hPa geopotential height difference fields for experiments g2aiso0, g2ens80-1, and g2chk0, respectively. The differences were computed with respect to the control experiment g2iso (black contour lines in the panels). Results are shown on AWIPS grid 212. Units are meters on all panels.

5. Summary and discussion

In this study, we have used an 80-member NCEP global ensemble to synthesize flow-dependent covariances in the GSI using recursive filters. A simple and plausible means for specifying the required ensemble-derived local aspect tensors has been presented. The experiments have been conducted using a lower-resolution version of the NCEP regional data assimilation system. The recursive filter generated covariances have been found to compare well with the exact covariances computed from the ensemble perturbation fields in the vicinity of selected anchor points. It is reiterated that, unlike in the exact ensemble covariances, the recursive filter generated covariances do not suffer from spurious correlations at long ranges. Furthermore, the use of a reduced 20-member ensemble was found to yield GSI covariances that differed little from those obtained with the original 80-member ensemble. The simplest, direct use of the ensemble as proposed in this study was found to result in rather weak anisotropies, which may be explained by the canceling effects of the averaging implied by the procedure. A remarkable improvement of the strength of the anisotropy was shown to be attainable by introducing a mean-field gradient-type term in the covariance construction, which in turn followed from the use of the surrounding grid points to artificially augment the size of the ensemble at the targeted grid point. A test case has been presented to evaluate the performance of the ensemble-based covariances. The best improvement to the 500hPa geopotential height forecast were found to come from the experiment with the strongest anisotropy following the artificial introduction of the mean-field gradient type term.

The results presented in this study have shown the potential for improving the NCEP forecast systems by using ensemble-derived background error covariances in the GSI. However, work is still needed. For example:

1. It is not clear what the relative contribution of the isotropic and anisotropic portions to the aspect tensor should be. The answer might be seasonally dependent, and long term experiments might be required to draw solid conclusions.
2. Cycling experiments covering a period of more than two weeks were found to lead to forecast skill scores that differed very little from those of the control experiment that used the default isotropic recursive filter (results not shown). These results may be pointing to the need for improving our specification of the ensemble-derived aspect tensors. On the other hand, they could also be pointing to the need to improve the balance constraint of the GSI, especially when anisotropic covariances are in use.
3. In the assimilation-forecast experiments reported in this work, the anisotropic covariances were only applied to stream function and velocity potential. Our final goal, however, is to be able to also apply adaptive covariances to temperature, moisture, and surface pressure. Preliminary experiments with additional anisotropic covariances applied to these variables showed little impact on the forecast. However, we believe that, together with improved balance relationships, a proper calibration of the covariance parameters will in the future lead to improved forecast results.
4. Similarly, the amplitudes of the covariance models used in the assimilation-forecast experiments reported in this work were based on the original variances from the default GSI isotropic filter. It is important to explore ways of incorporating the variance information from the ensemble to specify the filter amplitudes. Work along these lines is already in progress.
5. The impact of using a regional rather than a global ensemble merits investigations. Our current choice of the global ensemble has been dictated by the fact that the current NCEP regional ensemble uses several different models that display different characteristics among themselves. The best way to use such an ensemble in the context of building the covariances for data assimilation should be the subject of a separate study.
6. Testing experiments with the full-resolution NDAS are also desirable to ensure that our LR-NDAS is not "washing away" important small scale features that should be incorporated in the flow-dependent covariance construction.

References

Berre, L., O. Pannekoucke, G. Desroziers, S. E. Stefanescu, B. Chapnik and L. Raynaud 2007: A variational assimilation ensemble and the spatial filtering of its error covariances: increase of sample size by local spatial averaging. *Proceeding of ECMWF Workshop on Flow-dependent aspects of data assimilation*, 11-13 June 2007, 151-168.

Buehner, M. 2005: Ensemble-derived stationary and flow dependent background-error covariances: Evaluation in a quasi operational NWP setting. *Quart. J. Roy. Meteor. Soc.*, **131**, 1013-104

Daley, R. A. 1991: *Atmospheric Data Assimilation.* Cambridge University Press, 457 pp.

De Pondeca, M. S. F. V., R. J. Purser, D. F. Parrish, and J. C. Derber, 2006: Comparison of strategies for the specification of anisotropies in the covariances of a three-dimensional atmospheric data assimilation system. NOAA/NCEP Office Note 452, 13 pp.

Derber, J. C., and A. Rosati, 1989: A global ocean data assimilation system. *J. Phys. Ocean.,* **19**, 1333-1347.

Desroziers, G. 1997: A coordinate change for data assimilation in spherical geometry of frontal structure. *Mon. Wea. Rev.*, **125**, 3030-3038.

Hamill, T. M., and C. Snyder, 2000: A hybrid ensemble Kalman filter / 3D-variational analysis scheme. *Mon. Wea. Rev*., **128**, 2905-2919.

Hoskins, B. J., 1975: The geostrophic momentum approximation and the semigeostrophic equations. *J. Atmos. Sci.*, **32**, 233-242.

Hoskins, B. J., and F. P. Bretherton, 1972: Atmospheric frontogenesis models: mathematical foundation and solution. *J. Atmos. Sci.*, **29**, 11-37.

Hoskins, B. J., and I. Draghici, 1977: The forcing of ageostrophic motion according to the semigeostrophic equations and in an isentropic coordinate model. *J. Atmos. Sci.*, **34**, 1859-1867.

Liu, H., M. Xue, R. J. Purser, and D. F. Parrish: Retrieval of moisture from simulated GPS slant-path water vapor observations using 3DVAR with isotropic and anisotropic recursive filters. *Mon, Wea. Rev.,* **135**, 1506-1521.

Purser, R. J. , 2005: A geometrical approach to the synthesis of smooth anisotropic covariance operators for data assimilation. NOAA/NCEP Office Note 447, 60 pp.

Purser, R. J., W. –S. Wu, D. F. Parrish, N. M. Roberts 2003a: Numerical aspects of the application of recursive filter to variational statistical analysis, Part I: homogeneous and isotropic Gaussian covariance. *Mon. Wea. Rev.*, **131**, 1524-1535.

Purser, R. J., W. –S. Wu, D. F. Parrish, N. M. Roberts 2003b: Numerical aspects of the application of recursive filter to variational statistical analysis, Part II: spatially inhomogeneous and anisotropic general covariances. *Mon. Wea. Rev.*, **131**, 1535-1548.

Purser, R. J., M. S. F. V. De Pondeca, D. F. Parrish, and Dezső Dévényi 2007: Covariance modeling in a grid-point analysis. *Proceeding of ECMWF Workshop on flow-dependent aspects of data assimilation*, 11-13 June 2007, 11-25.

Riishøjgaard, L. P., 1998: A direct way of specifying flow-dependent background error correlations for meteorological analysis systems. *Tellus*, **50A**, 42-57.

Weaver, A., and P. Courtier, 2001: Correlation modeling on the sphere using a generalized diffusion equation. *Quart. J. Roy. Meteor. Soc.*, **127**, 1815-1846.

Wei, M., Z. Toth, R. Wobus, and Y. Zhu 2008: Initial perturbations based on the ensemble transform (ET) technique in the NCEP global operational forecast system. *Tellus*, **60A**, 62-79.

Wilks, D. W., 1995: *Statistical Methods in the Atmospheric Sciences*. Academic Press, San Diego, California, 467 pp.

Wu, W. –S, R. J. Purser, and D. F. Parrish 2002: Three-dimensional variational analysis with spatially inhomogeneous covariances. *Mon. Wea. Rev.*, **130**, 2905-2916.